

Received 28 June 2022, accepted 19 July 2022, date of publication 27 July 2022, date of current version 1 August 2022.

Digital Object Identifier 10.1109/ACCESS.2022.3194248

RESEARCH ARTICLE

Improved Complete Ensemble Robust Local Mean Decomposition With Adaptive Noise for Slewing Bearings Performance Degradation Assessment

YUBIN PAN¹, ZONGQIU HU², JIE CHEN¹, HUA WANG¹, AND RONGJING HONG¹

¹School of Mechanical and Power Engineering, Nanjing Tech University, Nanjing 211816, China

²China Three Gorges Construction Engineering Corporation, Chengdu 610041, China

Corresponding author: Jie Chen (chenjie_njtech@163.com)

This work was supported in part by the Project through the China Postdoctoral Science Foundation under Grant 2021M691558, in part by the Natural Science Foundation of Jiangsu Province under Grant BK20210547, in part by the Jiangsu Postdoctoral Research Grants Program under Grant 2021K297B, in part by the Science Research of Colleges Universities in Jiangsu Province under Grant 21KJB460036, and in part by the National Natural Science Foundation of China under Grant 51875273.

ABSTRACT Signal de-noising is one of challenging tasks in the slewing bearing performance degradation assessment due to the strong background noise and early weak fault characteristics. Adaptive digital driven methods like local mean decomposition (LMD) and robust local mean decomposition (RLMD) are a promising approach to implement signal-noise separation. However, the mode mixing problem limits its practical applications. Based on noise-assisted approach, complete ensemble robust local mean decomposition with adaptive noise (CERLMDAN) is used to solve this problem. Then, statistic detection of kernel principle component analysis (KPCA) is employed to select fault components for reconstruction and de-noising. After that, square prediction error (SPE) is utilized for performance degradation assessment model establishment. In the decomposition process of CERLMDAN, moth-flame optimization (MFO) is proposed to optimize the noise amplitude and ensemble trials for the improvement of signal decomposition ability. Meanwhile, a comparison is conducted between ensemble empirical mode decomposition (EEMD), variational mode decomposition (VMD), LMD, RLMD, CERLMDAN and MFO-CERLMDAN. The effectiveness of the proposed method is validated using numerical as well as experimental signals obtained through a slewing bearing highly accelerated life test. The results illustrate that MFO-CERLMDAN gets better result in signal de-noising, and SPE based on MFO-CERLMDAN-KPCA can assess the performance degradation of slewing bearing effectively.


INDEX TERMS Slewing bearing, performance degradation assessment, signal de-noising, CERLMDAN-KPCA, MFO.

I. INTRODUCTION

As a critical transmission component for wind turbine and tunnel boring machine, the reliability of slewing bearing has a serious impact on the safe operation of industry. Undetected small faults may degenerate into failure faults, even into major accidents. Therefore, accurate performance degradation assessment of slewing bearing can decrease unscheduled downtime and improve maintenance efficiency. However, due to the low speed and heavy load working conditions, vibration

signals collected from slewing bearings are corrupted with strong background noise [1]. For this reason, effective signal de-noising for performance degradation assessment is difficult but crucial.

The low signal-to-noise ratio (SNR) property causes difficulty and challenge on slewing bearing signal de-noising. Bearing faults usually start as small pits or spalls, and give sharp impulses in the early stages, and both fault types give rise to signals that can be treated as cyclostationary. However, one of the major sources of masking of the relatively weak bearing signals is strong frequency “noise” from hostile working conditions [2], [3]. Therefore, how to separate the

The associate editor coordinating the review of this manuscript and approving it for publication was Md. Moinul Hossain .

fault defect-related signal and background noise is of the first importance before proceeding with slewing bearing performance degradation assessment. Huang *et al.* [4] proposed empirical mode decomposition (EMD) to decompose signal into multiple intrinsic mode functions (IMF). However, EMD suffers from end effect and mode mixing problems [5], [6]. Ensemble EMD (EEMD) adds Gaussian white noise into raw signal many times, which effectively solves the problems of EMD [7], [8]. Moreover, the signal decomposition processed by EEMD is still corrupted with residual noise [9], [10]. To overcome the drawback, Torres *et al.* [11] proposed a self-adaptive signal decomposition method called complete ensemble empirical mode decomposition with adaptive noise (CEEMDAN). CEEMDAN gives an exact reconstruction of signals without mode mixing and with a better spectral separation [12], [13]. Recently, variational mode decomposition (VMD) and its derivative algorithm method is applied for the decomposition of time series data to eliminate the boundary effect as an advantage [14]–[18], but the disadvantage of VMD is that its number of decomposition levels is specified empirically [19]. Besides, a new local mean decomposition (LMD) method was proposed to analyze amplitude and frequency modulated signals [20], [21]. LMD product functions (PF) can retain more of the frequency and amplitude variation present in the original signal than is the case for the EMD IMFs. As an extension of LMD, Liu *et al.* [22] proposed robust LMD (RLMD), and RLMD is superior to traditional LMD in decomposition accuracy and time–frequency resolution [23]. However, RLMD still suffers from the mode mixing problem as LMD. Inspired by the previous studies presented in [11], [22], complete ensemble robust local mean decomposition with adaptive noise (CERLMDAN) method is proposed to address the existing problem of RLMD. However, the randomness of hyper parameter (noise amplitude and ensemble trials) is a major drawback of noise-assisted approach [24]. Moth-flame optimization (MFO), which is a relatively new intelligent optimization algorithm [25], has been widely applied in many field [26], [27]. Therefore, the proposed method named improved MFO-CERLMDAN exploits the merits of CERLMDAN approach to handle multiscale signals and the benefits of MFO method to handle parameter optimization. This makes the proposed method even more promising for facilitating the processing of nonlinear and non-stationary signals such as slewing bearing vibration signals.

After adaptive signal decomposition, another challenge in signal de-noising is how to establish an effective selection strategy of fault component [28]. The selection strategy for fault signal can be mainly divided into three types: (1) Calculate the characteristics of decomposed components, e.g. kurtosis [29], [30], power [31], permutation entropy [32], etc. (2) Calculate the difference between fault signal and its decomposed components, e.g. correlation coefficient [33]–[35]. (3) The fusion of above two strategies, e.g. kurtosis-correlation coefficient [36]–[38]. However, these indicators are easily affected by background noise

unrelated to fault or normal operation. Bakshi [39] put forward multiscale principal component analysis (MSPCA) method through calculating the PCA of wavelet coefficients at each scale decomposed by wavelet analysis. Due to its multiscale nature, MSPCA can extract those components which have specific signature for their standard condition that changes with the development of fault. However, how to choose wavelet basis function limits the application of wavelet analysis [40]. As an improvement of MSPCA, Feng *et al.* [41] utilized EEMD to decompose vibration signals, and employed PCA to select the most representative components throughout the life-cycle signals. However, PCA suffers from linear property, abandoning the information of higher-order statistics [42]. Zvokelj *et al.* [43] presented an EEMD-kernel PCA (KPCA) based de-noising and diagnosis approach for large-size bearings. Although EEMD eliminates the mode mixing of EMD, it easily falls into large reconstruction error. Therefore, based on the advantages of CERLMDAN and KPCA, we propose a nonstationary signal de-noising method using CERLMDAN-KPCA for slewing bearing. Hence, we adopted KPCA to select the PF whose behavior changes over time and frequency. Furthermore, vibration signal acquired from slewing bearing has strong nonlinearity and non-stationarity, which makes conventional feature extraction methods unavailable for health indicator construction. In this paper, square prediction error (SPE) based on KPCA is utilized for performance degradation assessment model establishment.

In view of the above-mentioned issues, we propose a performance degradation assessment methodology of slewing bearing based on MFO-CERLMDAN and KPCA. There are three steps in the proposed method. First, CERLMDAN optimized by MFO is employed to decompose the life-cycle vibration signals. Second, statistic detection of KPCA is employed to select fault PF components. Third, SPE is used to assess the performance degradation. The effectiveness of the proposed methodology has been validated using the experiment data collected from a slewing bearing life-cycle test. Experimental results illustrate that the proposed method provides a robust signal de-noising and feature extraction for enhanced performance degradation assessment capability. The main contributions of this work are summarized as follows:

- (1) Adaptive decomposition method (CERLMDAN) is employed to solve the mode mixing problem based on noise-assisted approach.
- (2) Parameter optimization of CERLMDAN using MFO makes the signal decomposition have high generalization performance and satisfactory stability. The proposed MFO-CERLMDAN outperforms the other five methods (EEMD, VMD, LMD, RLMD and CERLMDAN) in signal-noise separation, highlighting the superiority of parameter optimization.
- (3) A novel selection strategy based on KPCA is proposed to select fault PF components over life-cycle signals,

and SPE is utilized for performance degradation assessment model establishment.

The remainder of this paper is organized as follows: In Section II, LMD and RLMD are briefly described. CERLMDAN is introduced for the enhancement of adaptive signal decomposition. Section III outlines the systematic methodology of performance degradation assessment. In Section IV, the proposed method is validated on numerical and experimental signals obtained through a slewing bearing highly accelerated life test. The conclusion remarks of this paper and the recommendations for future research are presented in Section V.

II. METHODOLOGY

A. LMD

The essence of LMD is to decompose the non-stationary modulation signal into a series of PF components. Each PF component is formed by the product of an envelope signal and a pure FM signal. For a given signal $x(t)$, the detailed process of LMD is presented as follows [20]:

Step 1: Calculate the maximum and minimum n_i of signal $x(t)$, and obtain the local mean m_i and local magnitude a_i of each two successive extrema.

$$m_i = \frac{n_i + n_{i+1}}{2} \quad (1)$$

$$a_i = \frac{|n_i - n_{i+1}|}{2} \quad (2)$$

Step 2: Utilize the moving average method to obtain the local mean function $m_{11}(t)$ and envelope estimate function $a_{11}(t)$. Subtract local mean $m_{11}(t)$ the from $x(t)$.

$$h_{11}(t) = x(t) - m_{11}(t) \quad (3)$$

Step 3: Divide $h_{11}(t)$ by $a_{11}(t)$ to get the FM signal $s_{11}(t)$.

$$s_{11}(t) = \frac{h_{11}(t)}{a_{11}(t)} \quad (4)$$

Step 4: Repeat the above process for $s_{11}(t)$ to obtain the envelope function $a_{12}(t)$. The repeat implementation stops when $s_{1n}(t)$ is a pure FM signal, and obtain the envelope function $a_1(t)$ by multiplying all local envelope estimate functions.

$$a_1(t) = a_{11}(t)a_{12}(t) \dots a_{1n}(t) = \prod_{q=1}^n a_{1q}(t) \quad (5)$$

Step 5: Obtain the first PF₁ by multiplying $a_1(t)$ and FM signal.

$$\text{PF}_1(t) = a_1(t) s_{1n}(t) \quad (6)$$

Step 6: Get residual signal $u_1(t)$ through the subtraction of PF₁ from $x(t)$.

$$u_1(t) = x(t) - \text{PF}_1(t) \quad (7)$$

Step 7: Repeat the circulation implementation of Step 1~6. The iterative optimization stops when $u_k(t)$ is a constant

or contains no oscillations. Then, $x(t)$ can be decomposed into k PFs and a residual signal $u_k(t)$.

$$x(t) = \sum_{p=1}^k \text{PF}_p(t) + u_k(t) \quad (8)$$

B. RLMD

As described in Section II-A, boundary condition, envelope estimation, and sifting stopping criterion are three crucial aspects of LMD. As an improvement of LMD, RLMD can effectively improve all three aspects to improve the performance of LMD. The optimized process of RLMD can be listed as follows [22]:

Boundary conditions (update the Step 1 of LMD): Utilize the mirror extension algorithm [44] to determine the symmetrical points at the left and right ends of the signal, then calculate the local mean m_i and local magnitude a_i .

Envelope estimation (update the Step 2 of LMD): Employ a statistical method based on the statistics theory to automatically determine a reasonable fixed subset size for accurate envelope estimation. Then, the moving average algorithm is utilized as the smoothing algorithm of envelope estimation for the local mean function $m_{11}(t)$ and envelope estimate function $a_{11}(t)$.

Sifting stopping criterion (update the Step 4 of LMD): Within the repeat implementation, the objective function to describe the zero-baseline envelope signal is defined as

$$f = \text{RMS}(z(t)) + \text{EK}(z(t)) \quad (9)$$

where $z(t) = a(t) - 1$, i.e., the zero-baseline envelope signal.

$$\text{RMS}(z(t)) = \sqrt{\frac{1}{N_s} \sum_{t=1}^{N_s} z(t)^2} \quad (10)$$

$$\text{EK} = \frac{\frac{1}{N_s} \sum_{t=1}^{N_s} [z(t) - \bar{z}]^4}{\left(\frac{1}{N_s} \sum_{t=1}^{N_s} [z(t) - \bar{z}]^2\right)^2} - 3 \quad (11)$$

With the objective function, the proposed sifting stopping criterion is described as follows: For a sifting process of the i^{th} PF, $a_{ij}(t)$ is the smoothed local magnitude generated from the j^{th} iteration. In each iteration, the objective function value f_{ij} can be calculated by its definition in (9). The proposed sifting stopping criterion makes it decision depending on f_{ij} , f_{ij+1} , and f_{ij+2} obtained from three successive iterations. If $f_{ij+1} > f_{ij}$ and $f_{ij+2} > f_{ij+1}$, the sifting process stops and returns the corresponding results at the $(j - 1)^{\text{th}}$ iteration; otherwise, the sifting process continues until the iteration number reaches a predefined value that indicates the maximum iteration allowed in each sifting process.

C. CERLMDAN

RLMD is superior to traditional LMD in decomposition accuracy and time-frequency resolution. However, RLMD still

suffers from the mode mixing problem as LMD. As a result, CERLMDAN is utilized to address the existing problem of RLMD. Through adding a finite number of white noise in the decomposition process, CERLMDAN can give an exact reconstruction of signals without mode mixing and with a better spectral separation of the PFs. The procedure of CERLMDAN is briefly summarized as follows:

Step 1: Add white noise $\varepsilon_0\omega_i(t)$, $i = 1, 2, \dots, I$, to the raw signal $x(t)$ to obtain a new signal.

$$x_i(t) = x(t) + \varepsilon_0\omega_i(t) \quad (12)$$

where ε_0 is the noise amplitude and I denotes the ensemble trials.

Step 2: Implement RLMD for I times, and obtain the first PF₁. Subtract PF₁ the from $x(t)$ to get the first residual signal $u_1(t)$.

$$PF_1(t) = \frac{1}{I} \sum_{i=1}^I PF_{i1}(t) \quad (13)$$

$$u_1(t) = x(t) - PF_1(t) \quad (14)$$

Step 3: Implement RLMD for white noise $\omega_i(t)$ and set $R_j(\omega_i(t))$ as the j^{th} function of white noise, decomposed by RLMD. Add white noise $\varepsilon_1R_1(\omega_i(t))$ to the residual signal $u_1(t)$ to obtain a new signal $u_1(t) + \varepsilon_1R_1(\omega_i(t))$. Decompose $u_1(t) + \varepsilon_1R_1(\omega_i(t))$ until their first RLMD function, and get the second PF₂ and residual signal $u_2(t)$.

$$PF_2(t) = \frac{1}{I} \sum_{i=1}^I R_1(u_1(t) + \varepsilon_1R_1(\omega_i(t))) \quad (15)$$

$$u_2(t) = u_1(t) - PF_2(t) \quad (16)$$

Step 4: Repeat the circulation implementation as described in Step 2, and obtain the k^{th} PF_k and residual signal $u_k(t)$.

$$PF_k(t) = \frac{1}{I} \sum_{i=1}^I R_1(u_{k-1}(t) + \varepsilon_{k-1}R_{k-1}(\omega_i(t))) \quad (17)$$

$$u_k(t) = u_{k-1}(t) - PF_k(t) \quad (18)$$

Step 5: The iterative optimization stops when $u_k(t)$ is a constant or contains no oscillations. Then, $x(t)$ can be decomposed into k PFs and a residual signal $u_k(t)$.

$$x(t) = \sum_{p=1}^k PF_p(t) + u_k(t) \quad (19)$$

III. PERFORMANCE DEGRADATION ASSESSMENT BASED ON MFO-CERLMDAN-KPCA

A. PARAMETER OPTIMIZATION OF CERLMDAN USING MFO

Although CERLMDAN avoids the mode mixing compared with LMD and RLMD, the uncertainty of noise amplitude ε and ensemble trials I makes the signal decomposition prone to low generalization performance and unsatisfactory stability. The aim of adding white noise is to change the distribution of signal extreme points. Once white

noise makes the distribution most uniform, the decomposition accuracy of CERLMDAN reaches the highest. In other words, the smaller ε is, the less it can change the distribution of extreme points, which means white noise cannot play the role of uniform extreme point scale. Conversely, the larger ε will increase the number of decomposition and the amount of calculation. The ensemble trials I is utilized to reduce the influence of white noise. Although the increase of ensemble trials can reduce the decomposition error and improve the decomposition accuracy, it cannot be significantly improved when I increases to a certain extent. Consequently, the combination of noise amplitude ε and ensemble trials I in CERLMDAN are optimized by MFO for the improvement of signal decomposition ability.

1) ENVELOPE SPECTRUM ENTROPY

Information entropy has been widely employed to measure the instability of sample sequence. The more instable the system is, the higher the information entropy is, otherwise the opposite. Hence, vibration signals generated from a healthy bearing have a low impact energy, while that collected from a localized bearing damage have a high impact energy due to periodic impulsive excitations. For fault signal, impulsive excitation is relatively simple and stable, which means its information entropy is low. On the contrary, noise signal has strong randomness and complex components which has high information entropy. In view of this, envelope spectrum entropy is presented for the improvement of fault extraction in this paper. Through signal demodulation and Fourier transform, information entropy of envelope spectrum signal sequence can be obtained, which can better reflect the sparse characteristics of raw signal. The calculation formula of envelope spectrum entropy is:

$$H_e = - \sum_{j=1}^N q_j \log_2(q_j) \quad (20)$$

$$q_j = g(j) / \sum_{j=1}^N g(j) \quad (21)$$

where N is the number of samples. q_j is the normalization of envelope spectrum $g(j)$.

2) MFO

MFO is a random heuristic search algorithm based on swarm, which consider the lateral positioning of nocturnal moths as a source of inspiration. Set matrices \mathbf{M} and \mathbf{F} as the moths and flame, respectively. OM and OF store the fitness values of moths and flame, respectively. Moths are the actual search subjects moving in the search space, and flame is the best position obtained by moths. The update optimization process of MFO is as follows [25]:

After initializing the number and location of moth population, the update mechanism of moth population is as follows:

$$\mathbf{M}_i = S(\mathbf{M}_i, \mathbf{F}_j) = D_i^* e^{bt^*} \cos(2\pi t) + \mathbf{F}_j \quad (22)$$

where \mathbf{M}_i is the i^{th} moth, \mathbf{F}_j is the j^{th} flame, S is the spiral line function, $D_i = |\mathbf{F}_j - \mathbf{M}_i|$ is the distance between the i^{th} moth

and the j^{th} flame, b is a constant. In addition, t is random value $\in [r, 1]$, and r is the convergence constant linearly decreasing from -1 to -2 in the iterative update process.

To avoid falling into local optimization, the flames are sorted according to the fitness value to obtain an accurate global optimal solution after each iterative update. Then, the position of moths relative to the flame is updated, and the number of flames is adaptively reduced through (23).

$$\text{flame.no} = \text{round}\left(N - l * \frac{N - 1}{T}\right) \quad (23)$$

where N is the maximum number of flames, l is the current number of iterations, and T is the maximum iterations.

Compared with other swarm optimization algorithms, the biggest difference of MFO lies in that the particle search path is spiral, and the particles move around the better solution in a spiral way, rather than in a straight line. Therefore, MFO has strong parallel optimization ability, which can widely explore the search space and find the region with higher probability of global optimum.

3) OPTIMIZATION PROCESS OF MFO-CERLMDAN

The detailed optimization process for ε and I of CERLMDAN is summarized as follows:

Step 1: Implement parameter initialization of MFO, like the initial location, the population number of moth, number of iterations L , and the swarm population size;

Step 2: Update the population number of moth by (23);

Step 3: Train signal decomposition model, and set mean envelope spectrum entropy (MESE) as fitness function shown in (24). Then, MFO is employed to optimize the parameters of CERLMDAN, calculate the MESE of each moth M so as to find the optimal moth with the best fitness function, i.e. the flame F .

$$\text{MESE} = \frac{1}{k} \sum_{p=1}^k H_e(p) \quad (24)$$

Step 4: Update the position of moth in the search space by (22), calculate the corresponding fitness value of moth, and alter the order of flame according to the optimal solution;

Step 5: Repeat the circulation implementation of Step 2~4. The iterative optimization stops when the iterative number reaches the maximal iterative number or when the fitness function is no longer superior to global optimum. Then, output the optimal parameter combination (ε, I) , and establish the adaptive decomposition model.

B. STATISTIC DETECTION OF KPCA

Through calculating the contribution of each variable to the principal component, KPCA is mainly applied to feature dimensionality reduction. Besides, KPCA has been widely used to identify abnormal conditions of equipment. The main principle is to judge whether the signal is normal or not through comparing that whether the projection of sample space X in principal component subspace and residual subspace exceeds the threshold. Squared prediction error

(SPE) and Hotelling T^2 statistics are two common statistical detection methods. Considering that SPE statistics detection is more sensitive to abnormal condition than T^2 detection, this study utilizes KPCA-SPE statistics to identify abnormal condition.

$$\text{SPE} = \|\varphi(x), \varphi_k(x)\|^2 = \sum_{i=1}^n t_i^2 - \sum_{i=1}^k t_i^2 \quad (25)$$

where $\varphi(\cdot)$ is kernel function. n is the number of feature dimension, and k is the number of principal component. t_i is the projection in the i^{th} feature direction.

The threshold of SPE is given by:

$$\text{SPE}_{\text{lim}} = \theta_1 \cdot \left[\frac{c_\alpha h_0 \cdot \sqrt{2\theta_2}}{\theta_1} + 1 + \frac{\theta_2 h_0 (h_0 - 1)}{\theta_1^2} \right]^{1/h_0} \quad (26)$$

where c_α is the Gauss distribution of confidence level $(1 - \alpha)\%$. $h_0 = 1 - 2\theta_1\theta_3/3\theta_2^2$, $\theta_d = \sum_{j=k+1}^n \lambda_j^d$ ($d = 1, 2, 3$). λ_j is the j^{th} eigenvalue of covariance matrix of X .

C. PROPOSED PERFORMANCE DEGRADATION ASSESSMENT

After life-cycle signal decomposition by CERLMDAN, PFs contain the condition information of different frequency bands, where high-frequency PFs mainly contain noise and interference components, while low-frequency PFs include fault information. Hence, due to the uniformity of random white noise, high-frequency PFs change little at different periods of life cycle. Conversely, low-frequency PFs change obviously with the occurrence and aggravation of slewing bearing fault. Inspired by this point, we define a weighted cumulative value (WCV) of each PF during the entire life-cycle as a selection criterion to highlight the overall trend of each PF. Therefore, CERLMDAN-KPCA attempts to observe the change trend of each PFs in the whole life cycle, and then selects PFs which can best assess the performance degradation of slewing bearing. The detailed de-noising procedure is listed as follows:

Step 1: Divide life-cycle vibration signal $a(t)$ into K segments, $a_k(t)$ is the k^{th} segment of $a(t)$. ($k = (1, 2, \dots, K)$). $a_1(t)$ represents the healthy signal under the normal operation of slewing bearing.

Step 2: Implement CERLMDAN on each segment and obtain H PFs, define the PF_{hk} as the h^{th} PF of $a_k(t)$ ($h = (1, 2, \dots, H)$).

Step 3: Split PF_{hk} into multi-dimensional matrix \mathbf{G}_{hk} , which is defined by (27).

$$\mathbf{G}_{hk} = \begin{matrix} m = \frac{L}{i} \\ = \begin{bmatrix} \text{PF}_{hk,1} & \text{PF}_{hk,2} & \dots & \text{PF}_{hk,m} \\ \text{PF}_{hk,m+1} & \text{PF}_{hk,m+2} & \dots & \text{PF}_{hk,2m} \\ \vdots & \vdots & \vdots & \vdots \\ \text{PF}_{hk,(i-1)m+1} & \text{PF}_{hk,(i-1)m+2} & \dots & \text{PF}_{hk,L} \end{bmatrix}, \end{matrix} \quad (27)$$

where i is the dimension of G_{hk} , and set as 4 in this paper. L is the length of PF_{hk} .

Step 4: Set the first matrix G_{h1} as the healthy KPCA model, and map G_{hk} into G_{h1} getting the SPE_{hk} statistics and root mean square R_{hk} of SPE_{hk} . Hence, S_{hk} , obtained by using the subtraction of R_{h1} from R_{hk} , is defined as the indicator of the change comparing each PFs of a_k with a_1 .

Step 5: Calculate the WCV of S_{hk} , which is defined by (28). Obviously, the larger WCV_h is, the more sensitive the PF_h of a_k is, which has a larger anomaly over time and can represent the degradation component of this signal.

$$WCV_h = \sum_{k=2}^K \left(S_{hk} \times S_{hk} / \sum_{i=1}^H S_{ik} \right) \quad (28)$$

where $\sum_{i=1}^H S_{ik}$ is the cumulative value of H PFs at the k^{th} segment. The square of S_{hk} is to emphasis on changing trends of the h^{th} PF.

Step 6: Select the PFs of each segment which have larger WCV proportion, and obtain the reconstructed signal $a^R(t)$. For a clear presentation of CERLMDAN-KPCA, the de-noising process is depicted in Fig. 1.

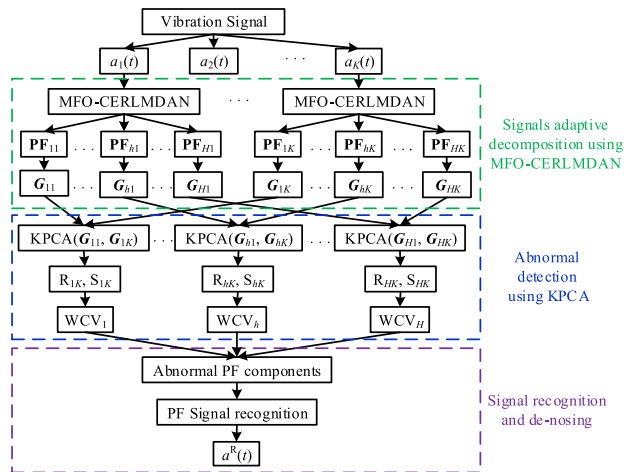


FIGURE 1. Procedure of the proposed de-noising method.

After life-cycle signal de-noising, SPE statistics are utilized as health indicator to access the performance degradation. The performance degradation assessment procedure is shown in Fig. 2. After signal de-noising, the n^{th} ($n = [1, N]$) segments of the de-noised vibration signal $a^R(t)$ is split into multi-dimensional matrix G_n . Set the first matrix G_1 as the healthy KPCA model, then G_1, G_2, \dots, G_N are projected onto the healthy KPCA model to obtain SPE statistics ($SPE_1, SPE_2, \dots, SPE_N$). By connecting every SPE, SPE is then acquired to reveal the change of the vibration signal relative to the normal condition. The flowchart of the proposed method is shown in Fig. 3.

Besides, it should be noted that most of the existing signal de-noising methods deal with signals with a few seconds or

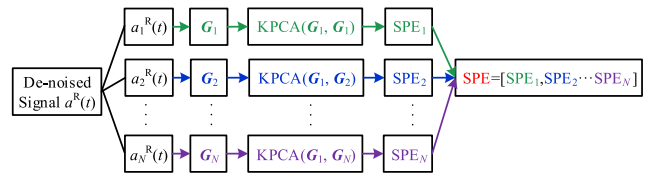


FIGURE 2. Health indicator construction.

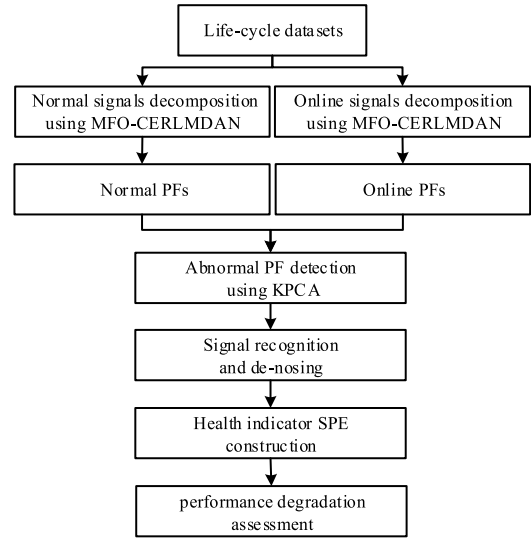


FIGURE 3. Flowchart of the proposed method.

even shorter duration. Conversely, this method aims at the whole life vibration signal, which can more accurately extract the components that assess the performance degradation of slewing bearing. Hence, it can be observed from the above steps that this method can adaptively adjust the parameters in the process of signal decomposition, fault component selection and health indicator construction according to raw signal characteristics. The whole signal de-noising can be implemented without human intervention, which avoids the tedious hand-crafting parameters in the existing methods.

IV. NUMERICAL VALIDATION AND EXPERIMENTAL ANALYSIS

A. NUMERICAL VALIDATION

To validate the effectiveness of the proposed CERLMDAN, a numerical test is implemented for comparison. However, there is no relevant standard or widely accepted numerical equation for slewing bearing. Considering the structural similarity with common bearing, a series of periodic exponential decaying high frequency oscillation is utilized to simulate the impact signal produced by bearing local fault [45]. The numerical signal can be described as:

$$x(t) = e^{-bt_1} \sin(2\pi f_c t) \quad (29)$$

$$t_1 = \text{mod} \left(t, \frac{1}{f_m} \right) \quad (30)$$

where b is the exponential frequency. f_c represents the carrier frequency. f_m denotes the modulation frequency.

The parameters used in (29) and (30) are as follows: the exponential frequency $b = 800$, the carrier frequency $f_c = 1500$ Hz. The modulation frequency f_m is 10 Hz. Numerical signal is generated by (29) and (30) with a sampling time $t = 0 \sim 0.01$ s and sampling frequency 100 kHz. The numerical time series waveforms of bearing fault signal and random noise are shown in Fig. 4(a) and Fig. 4(b), respectively. Then, random noise is added to the bearing fault signal, as illustrated in Fig. 5. From Fig. 5, it can be obviously observed that fault signal with noise is completely submerged by noise. As a result, MFO-CERLMDAN signal-noise separation method is implemented on the numerical bearing fault signal.

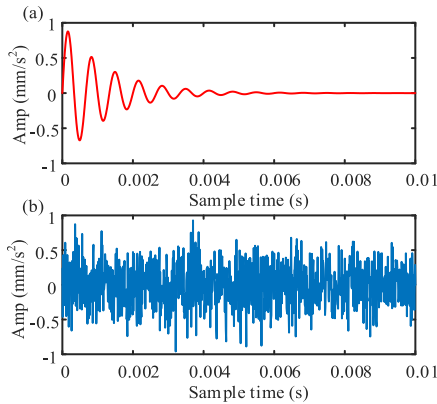


FIGURE 4. Waveforms of numerical signals: (a) Bearing fault signal, (b) Random noise.

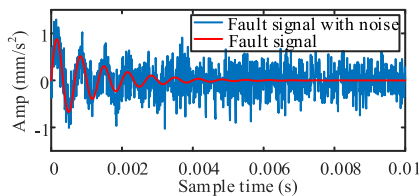


FIGURE 5. Waveforms of numerical bearing fault signal with noise.

For the ease of understanding, only LMD, RLMD and non-optimization CERLMDAN are tested to illustrate the de-noising effect of MFO-CERLMDAN. The decomposition parameters noise amplitude and ensemble trials of non-optimization CERLMDAN suggested by Wu and Huang [7] are set as 0.2 and 100, respectively. To enhance the ability of decomposition, MFO is employed to optimize the decomposition parameters of CERLMDAN. The noise amplitude ε search interval [0.01, 0.5], ensemble trials I search interval [1, 200].

Then, the fault signal with noise is decomposed using LMD, RLMD, and non-optimization CERLMDAN shown in Fig. 6. Through the optimization iteration as shown in Fig. 7(a), noise amplitude and ensemble trials of MFO-CERLMDAN are set as 0.2387 and 101, respectively. The decomposition result of MFO-CERLMDAN is depicted in Fig. 7(b). From Fig. 6 and Fig. 7, a series of PFs with different frequency bands from high to low are obtained by

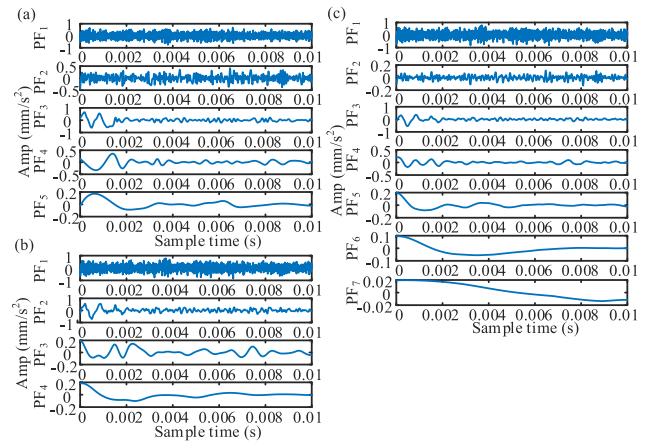


FIGURE 6. PFs of different methods: (a) LMD, (b) RLMD, (c) CERLMDAN.

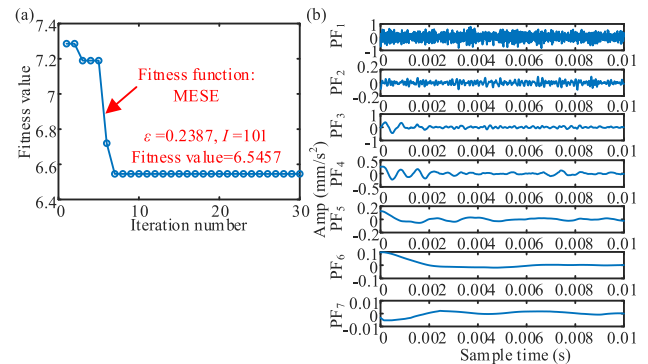


FIGURE 7. Decomposition of MFO-CERLMDAN: (a) Iteration result, (b) PF.

four kinds of methods, and there exists some differences for different decomposition methods. It can be observed that PFs decomposed by LMD and RLMD are less than CERLMDAN related methods owing to the noise-assisted influence. The high-frequency noise are concentrated in the component PF₁, while the fault-related components mainly exist in PF₂ of RLMD and PF₃ of LMD, non-optimization CERLMDAN and MFO-CERLMDAN. However, compared with RLMD, the imaginary component PF₂ is generated by LMD. Hence, the first two attenuation oscillations in PF₃ of LMD and PF₂ of RLMD show obvious mode mixing. On the contrary, this phenomenon is smoothed out by non-optimization CERLMDAN and MFO-CERLMDAN. Although the addition of noise leads to the generation of imaginary component (PF₂ of non-optimization CERLMDAN and MFO-CERLMDAN), the amplitude of imaginary component is obviously lower than that of LMD. Therefore, it is reasonable to conclude that the CERLMDAN related methods indicates a good performance in the adaptive signal decomposition.

For simplicity, the decomposed PFs based on the proposed method with kurtosis criterion is given in Table 1. It is found that PF₂ ~ PF₅ of LMD, PF₂ ~ PF₄ of RLMD, PF₂ ~ PF₆ of non-optimization CERLMDAN and PF₂ ~ PF₇ of MFO-CERLMDAN are determined as fault-related PFs according to kurtosis criterion, which are greater than 3. By means of the

TABLE 1. Kurtosis index of decomposed PFs.

Decomposition methods	PF1	PF2	PF3	PF4
LMD	2.1748	3.0580	6.7890	5.6760
RLMD	2.5554	6.3188	4.1014	5.5080
CERLMDAN	2.5641	3.5834	9.5913	5.7553
MFO-CERLMDAN	2.5812	3.4728	8.2850	6.0738
Decomposition methods	PF5	PF6	PF7	
LMD	5.0406	—	—	
RLMD	—	—	—	
CERLMDAN	10.0880	3.0498	1.7399	
MFO-CERLMDAN	8.1841	7.4643	4.3923	

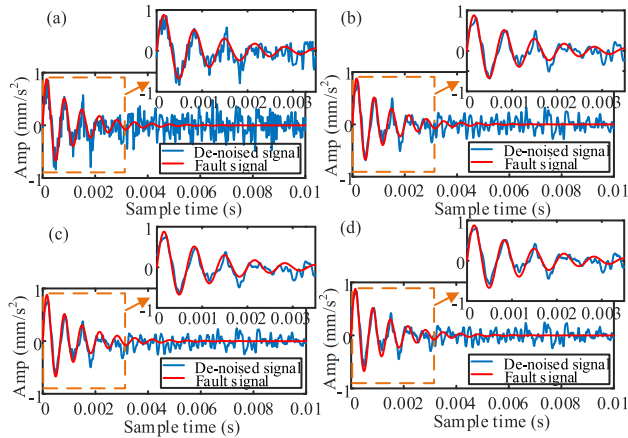


FIGURE 8. De-noised signals: (a) LMD, (b) RLMD, (c) CERLMDAN, (d) MFO-CERLMDAN.

decomposition and reconstruction through these four methods, Fig. 8 shows the comparison of de-noised fault signals. The orange dotted rectangular region is enlarged as shown in Fig. 8. It can be observed that these four methods can remove the majority of the noise, making the fault features which are submerged in noise clearer. Among these four methods, LMD shows the worst de-noising effect either at the wave crest or later stable period. By the improvement of three crucial aspects, RLMD removes the majority of noise than LMD. Based on noise-assisted approach, CERLMDAN provides better signal de-noising in comparison to RLMD, especially at the third wave crest and late stable period. The main reason to explain this phenomenon is the mode mixing problem of LMD and RLMD, which affects the signal decomposition effect. MFO-CERLMDAN has the same high accuracy with CERLMDAN, but impact components are mined more obviously by MFO-CERLMDAN from a detailed observation of the fourth and fifth wave crest. Besides, the other two methods EEMD and VMD are carried out for the comparison. Fig. 9 shows the de-noised results of EEMD and VMD. Although these two methods also have the ability to remove the majority of noise, the wave crest and later stable period exist strong noise interference compared with LMD-related methods. In summary, the proposed MFO-CERLMDAN has a merit of accurate signal de-noising, highlighting the superiority of parameter optimization.

To quantitatively evaluate the performance of each method in signal de-noising, the mean squared error (MSE) and

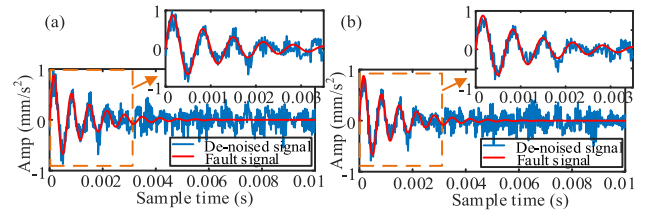


FIGURE 9. De-noised signals: (a) EEMD, (b) VMD.

SNR are calculated to carry out the comparison. MSE is employed to measure the deviation between de-noised and raw signal, while SNR is utilized to determine the ratio of noise level added to the signal. In other words, the smaller MSE is, the lower de-noised error is, and the larger SNR is, the lower the noise level is, which can represent the stronger de-noising effect. The mathematical expression of MSE and SNR are as follows:

$$MSE = \frac{1}{m} \sum_{i=1}^m (x_i - \hat{x}_i)^2 \quad (31)$$

$$SNR = 10 \log_{10} \left(\frac{\sum x_i^2}{\sum (x_i - \hat{x}_i)^2} \right) \quad (32)$$

where x_i is the signal without noise. \hat{x}_i represents the de-noised signal. m denotes the number of samples.

The MSE and SNR of de-noised signal based on EEMD, VMD, LMD, RLMD, non-optimization CERLMDAN and MFO-CERLMDAN are listed in Table 2. Although EEMD and VMD perform better than LMD, RLMD is superior to these two methods owing to the elimination of mode mixing. However, the de-noising effect of RLMD is worse than CERLMDAN-related methods which are based on noise-assisted approach. Among these six methods, the MSE of MFO-CERLMDAN are slightly lower, while the SNR is higher, which means that the proposed method can effectively improve the decomposition efficiency, suppress noise and make the de-noised signal closer to the raw fault vibration signal. Therefore, these results show that the proposed MFO-CERLMDAN outperforms the other five methods in signal-noise separation in our case study.

TABLE 2. Evaluating indicator of de-noised signals.

Decomposition methods	MSE	SNR
EEMD	0.0233	1.2318
VMD	0.0187	2.1930
LMD	0.0285	0.3643
RLMD	0.0152	3.0902
CERLMDAN	0.0117	4.2261
MFO-CERLMDAN	0.0107	4.6149

B. EXPERIMENTAL ANALYSIS

1) SLEWING BEARING TEST RIG

The slewing bearing test rig is designed to simulate the life-cycle operation under the actual working condition. Fig. 10 shows the line diagram of designed slewing bearing test rig. The main test slewing bearing linked with accompanied slewing bearing through the bolt. The combination

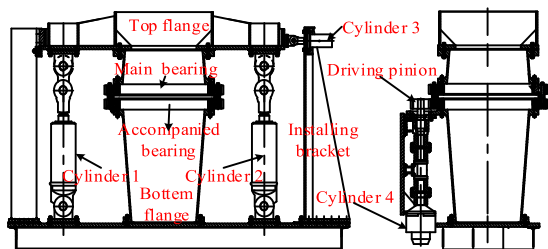


FIGURE 10. The structural diagram of slewing bearing test rig.

of cylinder 1 and cylinder 2 provides the axial force and overturning moment. Cylinder 3 exerts radial force, which is transferred to slewing bearing via top flange. Hence, slewing bearing is driven by hydraulic motor cylinder 4. The physical map of slewing bearing test rig is shown in Fig. 11. The key parameters of slewing bearing test rig are listed in Table 3.

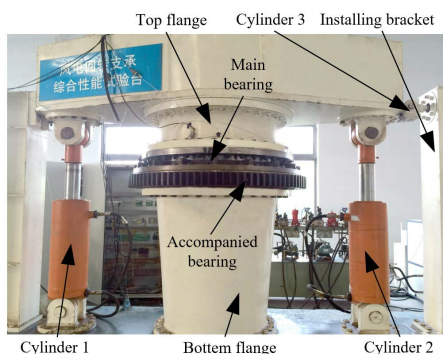


FIGURE 11. Physical map of slewing bearing test rig.

TABLE 3. Parameters of slewing bearing test rig.

Parameters	Value
Axial force (kN)	0-750
Radial force (kN)	0-101.8
Overturning moment (kN·m)	0-880
Rotational speed (r/min)	0.5-5
Diameter of slewing bearing (mm)	600-2 000

To accelerate the test as much as possible, the limiting operating condition load of slewing bearing is applied to the test. The test slewing bearing used in the accelerated life-cycle test is QNA-730-22 shown in Fig. 12 and its structure is homologous to the single-row four-point contact ball structure with inner gear. Table 4 shows the parameters of test slewing bearing. Hence, the test speed is suggested as rated operating condition speed of 4 rpm.

Generally, the slewing bearing is mainly subjected to the combination force of axial force, radial force and overturning moment as shown in Fig. 13(a). Hence, to avoid repeated quenching caused by raceway heat treatment, there must be an untreated area in the raceway, namely, soft belt. Meanwhile, according to the load distribution, the soft belt should be installed at the position with small bearing capacity as far as possible. Therefore, four accelerometer sensors are mounted at every 90 degree measuring interval as shown in Fig. 13(b).



FIGURE 12. Test slewing bearing.

TABLE 4. Parameters of test slewing bearing.

Parameters	Value
Raceway diameter(mm)	730
Ball diameter(mm)	22
Contact angle(°)	45
Curvature ratio	1.06
Number of the ball	91

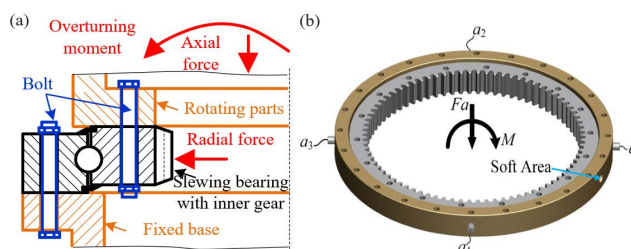


FIGURE 13. Structure and distribution of acceleration sensors: (a) Structure diagram, (b) Acceleration sensors installation position.

The life-cycle test was stopped when the slewing bearing was stuck and a failure occurred. The slewing bearing raceway, ball and cage condition at the end of the test are shown in Fig. 14. The spalling damage not only happened to inner raceway, but also at the outer raceway, especially in the soft belt area. Meanwhile, more stretch pitting and stretch marks were formed in the ball and cage with the long-term cyclic contact load.

To reflect the condition of slewing bearing, the vibration signals of vibration sensors are collected. Taking into consideration the maintenance of test rig, only 11 days vibration signals are extracted as shown in Fig. 15. From Fig. 15, we can observe that there exists an increasing trend in the amplitude of vibration signals as the fault deteriorates. However, due to background noise in the raw time series data, not much fault information can be extracted from the vibration signal. Therefore, the proposed MFO-CERLMDAN-KPCA is applied to signal de-noising according to the procedure shown in Fig. 1.

2) DATA PROCESSING AND ANALYSIS

The raw time series signal is first divided into 11 segments according to the test time. We calculate the PFs of each segment by performing MFO-CERLMDAN. Taken the severe fault period as sample, different PFs decomposed by these three methods (LMD, RLMD and CERLMDAN) are shown in Fig. 16. According to parameter optimization by MFO as shown in Fig 17(a), noise amplitude and ensemble trials of CERLMDAN are set as 0.1370 and 149,

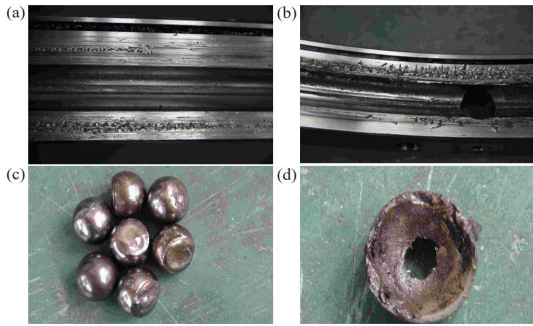


FIGURE 14. Damage components of slewing bearing: (a) Inner raceway, (b) Outer raceway, (c) Ball, (d) Cage.

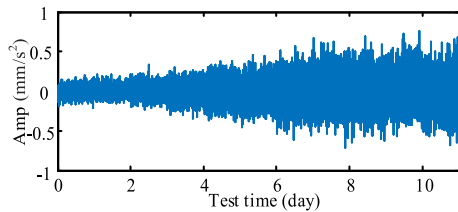


FIGURE 15. Test vibration signals.

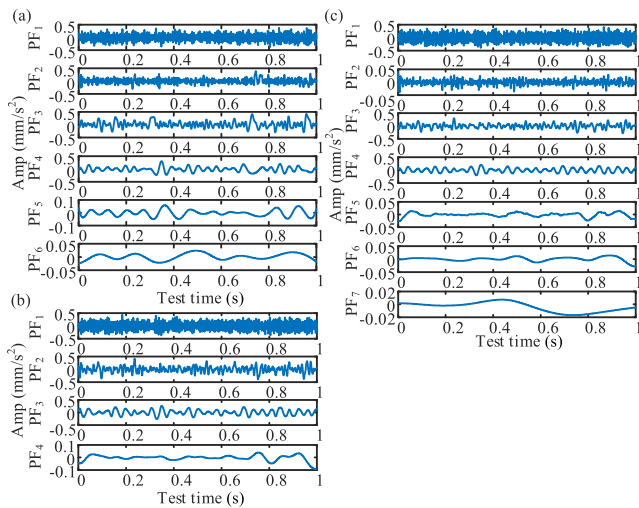


FIGURE 16. PFs of different methods: (a) LMD, (b) RLMD, (c) CERLMDAN.

that the involved method makes a satisfactory performance. The decomposition result of MFO-CERLMDAN is depicted in Fig. 17(b). From Fig. 16 and Fig. 17, the following conclusions can be summarized: (1) the imaginary component PF₂ is generated by LMD, while this phenomenon does not happen to RLMD; (2) Although the addition of noise leads to the increase of PF components, mode mixing is smoothed out by non-optimization CERLMDAN and MFO-CERLMDAN; (3) Compared with non-optimization CERLMDAN, especially in PF₂, the decomposition results of the proposed MFO-CERLMDAN have the highest accuracy because it further strengthens the decomposition ability under the suitable adaptive noise and ensemble trials. Through the comparison of different decomposition methods, it is

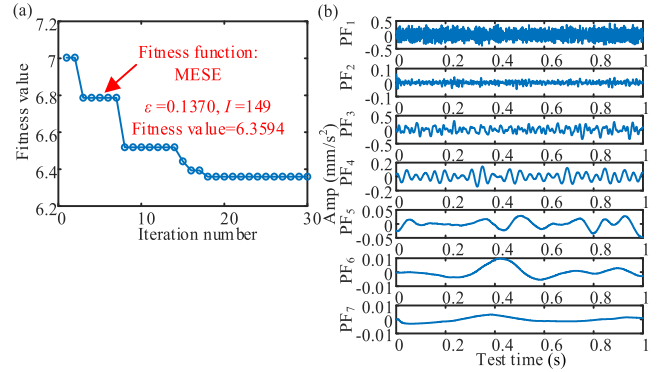


FIGURE 17. Decomposition of MFO-CERLMDAN: (a) Iteration result, (b) PF.

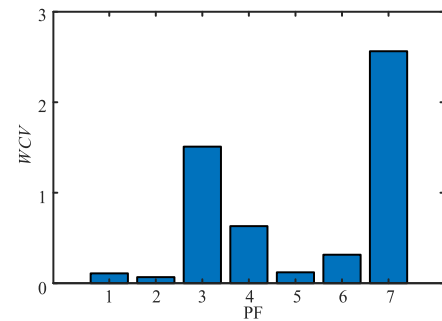


FIGURE 18. PF selection of MFO-CERLMDAN-KPCA.

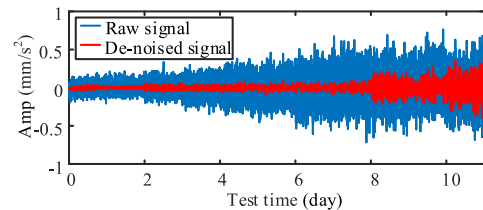


FIGURE 19. De-noised vibration signal of MFO-CERLMDAN-KPCA.

observed that MFO-CERLMDAN obtains the best model for signal-noise separation of slewing bearing.

After life-cycle signal decomposition, fault component selection is carried out. For simplicity, only the selection procedure of MFO-CERLMDAN is presented as below and the de-noising effectiveness is compared with the other three approaches. To obtain more accurate changes for each PF, the WCV of each PF is calculated. Fig. 18 shows the results. It can be seen that the 3th, 4th and 7th PFs have a higher proportion in all PFs. Then, these three PFs are selected to reconstruct the signal. The raw and de-noised signals using the MFO-CERLMDAN-KPCA are shown in Fig. 19.

To validate the superiority of MFO-CERLMDAN-KPCA, LMD-KPCA, RLMD-KPCA and CERLMDAN-KPCA are utilized to de-noise the vibration signals for the comparison. Fig. 20 shows the de-noised results of the other three de-noised methods, highlighting that a considerable white noise reduction can be achieved with accurate signal decomposition and proper PFs selection which contain the sensitive

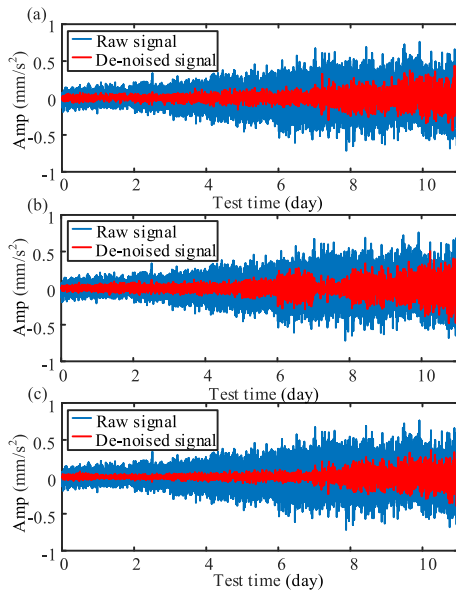


FIGURE 20. De-noised vibration signals: (a) LMD-KPCA, (b) RLMD-KPCA, (c) CERLMDAN-KPCA.

fault information. It is clear that the proposed method MFO-CERLMDAN-KPCA (Fig. 19) and CERLMDAN-KPCA (Fig. 20(c)) shows the performance degradation information more clearly, while that in LMD-KPCA (Fig. 20(a)) and RLMD-KPCA (Fig. 20(b)) de-noised signal seem to be buried in background noise, especially at the early and later period of LMD-KPCA, and middle period of RLMD-KPCA. It can be observed from Fig. 19 and Fig. 20(c) that there is an obvious fluctuation in amplitude around at early period, indicating a running-in process in health status of the slewing bearing. However, such an increase is not visible in Fig. 20(a) and Fig. 20(b). Moreover, MFO-CERLMDAN-KPCA provides better signal de-noising in comparison to CERLMDAN-KPCA from an overall trend observation.

After the comparison of KPCA with different decomposition methods, MFO-CERLMDAN can effectively improve de-noising accuracy. However, the above analysis only focus on LMD-related decomposition method. Therefore, another issue with adaptive signal de-noising are related to how different common decomposition methods influence the accuracy of signal de-noising. For the purposes of the comparison, another two methods are selected to validate the effectiveness of the proposed MFO-CERLMDAN-KPCA based de-noising model: EEMD and VMD. To conduct a fair comparison, KPCA is utilized as the fault selection strategy for EEMD and VMD. Fig. 21 shows the comparison of de-noised signals. It can be observed that performance degradation information is not visible in the severe fault period of EEMD-KPCA, and the middle period of VMD-KPCA is occupied by noise. Therefore, the results illustrate that the proposed de-noising method MFO-CERLMDAN-KPCA has a better de-noising effect on such low signal-to-noise vibration signals.

After the signal de-noising of vibration signal, SPE statistics are utilized as health indicator to access the performance

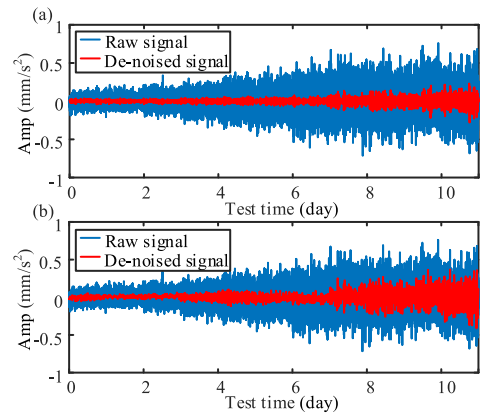


FIGURE 21. De-noised vibration signals: (a) EEMD-KPCA, (b) VMD-KPCA.

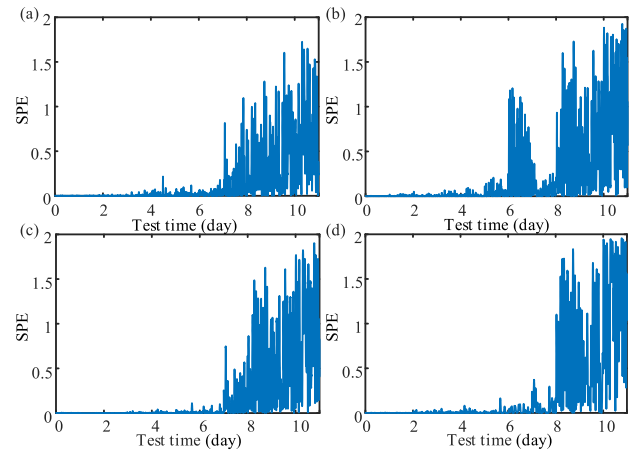


FIGURE 22. Health indicator SPE: (a) LMD-KPCA, (b) RLMD-KPCA, (c) CERLMDAN-KPCA, (d) MFO-CERLMDAN-KPCA.

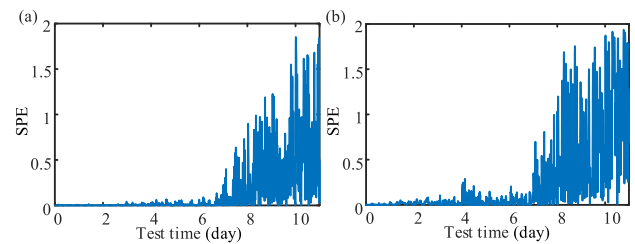


FIGURE 23. Health indicator SPE: (a) EEMD-KPCA, (b) VMD-KPCA.

degradation. According to the flowchart shown in Fig. 2, Fig. 22 and Fig. 23 depicts the health indicator SPE of different de-noised signals. The health indicator is more sensitive to the performance degradation of slewing bearing, and SPE intuitively presents the overall progression of health degradation compared with raw vibration signal. However, there exists abnormal fluctuation at fifth day of LMD-KPCA and RLMD-KPCA. Conversely, SPE of CERLMDAN-KPCA and MFO-CERLMDAN-KPCA remain stable until the seventh day of abnormal rise. It should be noted the slewing bearing was dismantled and maintained at the seventh day due to the abnormal sound, which can explain the abnormal rise. However, the maintenance is not reflected

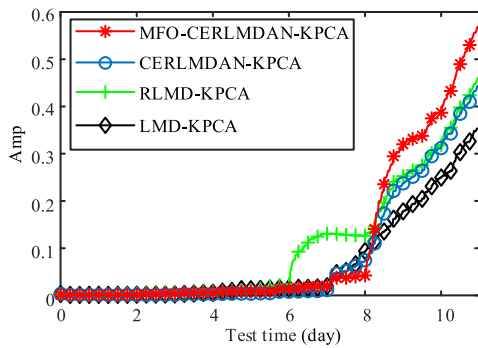


FIGURE 24. RMS of different LMD-related de-noised methods.

in the SPE trend of CERLMDAN-KPCA. Besides, same as de-noised signals, the amplitude of EEMD-KPCA is lower than MFO-CERLMDAN-KPCA, and there exists a sharp rise in VMD-KPCA at the fifth day. Therefore, Fig. 22 and Fig. 23 highlight that the SPE feature of MFO-CERLMDAN-KPCA has the ability to accurately assess the performance degradation of slewing bearing.

It can be observed that SPE is utilized to reflect the data difference between normal signals with online operation signals. The calculated value of SPE is non-negative, and there are no spectral characteristics of SPE. To further reflect the ability of performance degradation assessment, time domain feature is extracted from SPE of different signal de-noising methods for the comparison. The widely used time domain feature is root mean square (RMS), and it is sensitive to progressive deterioration assessment. As a result, the trend of RMS extracted from SPE of de-noised signals as shown in Fig. 24. It can be observed that all the extracted RMS depict a significant increase in amplitude over the life cycle of slewing bearing and thus reflect its degradation trend. However, there are many differences in the trend of each RMS. RMS extracted from LMD-KPCA has the lowest amplitude at the late period, which means that its de-noised effect is the worst. Hence, there exists an obvious abnormal rise of RLMD-KPCA, which is consistent with the observation in Fig. 20(b). Among these four methods, RMS of MFO-CERLMDAN-KPCA shows a steady trend at the early-middle period, while the amplitude is highest at the late period, which means that the proposed method can capture overall degradation of slewing bearing. Fig. 25 shows the comparison of different traditional de-noised methods. EEMD-KPCA has the lowest amplitude at the late period, while VMD-KPCA exists abnormal rise at the second day. After the comparison of different methods, it is concluded that RMS of SPE with MFO-CERLMDAN-KPCA obtains the best model for performance degradation assessment of slewing bearing.

After the comparison of different methods, MFO-CERLMDAN-KPCA is even more promising for facilitating the process of slewing bearing signal de-noising. To further emphasize the significance of signal de-noising, RMS of SPE based on raw signal is selected to validate the effectiveness of the proposed MFO-CERLMDAN-KPCA de-noising model.

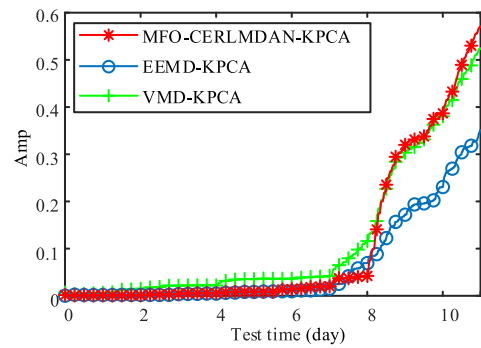


FIGURE 25. RMS of different traditional de-noised methods.

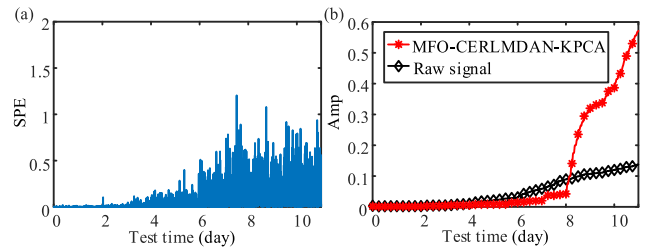


FIGURE 26. SPE and its RMS of raw signal: (a) SPE, (b) RMS.

Fig. 26(a) shows the health indicator SPE based on raw signal, and Fig. 26(b) illustrates the RMS of SPE. From Fig. 26, the following conclusions can be summarized: (1) Although the amplitude of raw vibration signal is larger than de-noised vibration signals shown in Fig. 19, SPE of raw vibration signal is lower than that of de-noised signals. The reason to explain this phenomenon is that the fault of slewing bearing is submerged by noise before signal de-noising, resulting in poor detection effect. (2) The SPE and its RMS extracted from raw signal rises at the fourth day, which is inconsistent with the degradation process of slewing bearing. Therefore, the implementation of MFO-CERLMDAN-KPCA signal de-noising cannot make the fault characteristics which are submerged in noise clearer, but also substantially improve the accuracy of performance degradation assessment.

The main reason to explain good performance of our proposed method is the signal decomposition strategy of MFO-CERLMDAN, which can avoid mode mixing based on noise-assisted approach and parameter randomness based on swarm optimization algorithm. However, different from noise-assisted approach of CERLMDAN-related methods, the decomposed components of LMD suffer from mode mixing. Although RLMD is superior to traditional LMD in decomposition accuracy and time-frequency resolution, it still has the same problem with LMD. Conversely, CERLMDAN, which has a great performance using noise-assisted approach, may bring into a less optimal spectral separation with the inappropriate combination of decomposition parameters.

To sum up, the research emphasis of the proposed method includes: (1) Adaptive signal decomposition: Based on noise-assisted approach, CERLMDAN can generate PFs with

the proper scale and less residual noise, and solve the mode mixing problem. MFO can capture parameters combination as appropriate as possible, which ensures high decomposition accuracy. (2) Effective fault component selection: Under the premise of high decomposition accuracy, another factor of signal de-noising depends on fault component selection strategy. In view of life-cycle vibration signals, statistic detection of KPCA can extract those components which have specific signature for their standard condition that changes with the development of fault. Therefore, the combination of MFO-CERLMDAN and KPCA method highlights high performance, which makes this method more suitable for slewing bearing performance degradation assessment.

V. CONCLUSION

This paper presents a novel performance degradation assessment methodology based on improved CERLMDAN. The proposed method is used for the large-size low-speed slewing bearing. The life-cycle vibration signals from a slewing bearing highly accelerated life test are analyzed to validate the superiority of the proposed method. Based on noise-assisted approach, CERLMDAN outperforms the LMD and RLMD in signal-noise separation. To avoid the randomness of hyper parameters in CERLMDAN, the combination of noise amplitude and ensemble trials in CERLMDAN is optimized by MFO for the improvement of signal decomposition ability. Hence, the accuracy of numerical signal de-noising based on MFO-CERLMDAN is superior to the other two traditional decomposition methods EEMD and VMD. In this paper, four LMD-related life-cycle signal de-noising methods are analyzed: LMD-KPCA, RLMD-KPCA, CERLMDAN-KPCA and MFO-CERLMDAN-KPCA. Moreover, EEMD-KPCA and VMD-KPCA are presented to further emphasize the effectiveness of the proposed method. The experiment results demonstrate that the proposed MFO-CERLMDAN with KPCA cannot only improve the signal decomposition accuracy, but also select the most representative components throughout the life-cycle signals. In terms of feature extraction, SPE based on MFO-CERLMDAN-KPCA can assess the performance degradation of slewing bearing compared with the other five methods.

Besides, maintenance plans based on health condition division can shorten maintenance intervals, thus reduce maintenance costs. However, there is no uniform criterion for judging life conditions of slewing bearing. Future works will focus mainly on how to set failure threshold according to health indicator. Meanwhile, how to improve the computational efficiency of parameter optimization in CERLMDAN should be explored further. Furthermore, this numerical validation can be considered as the first investigative step since it concerns a single exponential decaying high frequency oscillation and therefore its effectiveness of a multi-component example has to be proved with further investigations. Also, the future work will mainly focus on the development of online assessment system, making it convenient for the application in actual engineering to realize the worry-free industry.

REFERENCES

- [1] Y. Pan, R. Hong, J. Chen, Z. Qin, and Y. Feng, "Incipient fault detection of wind turbine large-size slewing bearing based on circular domain," *Measurement*, vol. 137, pp. 130–142, Apr. 2019.
- [2] R. B. Randall and J. Antoni, "Rolling element bearing diagnostics—A tutorial," *Mech. Syst. Signal Process.*, vol. 25, no. 2, pp. 485–520, 2011.
- [3] Q. Ni, J. Ji, and K. Feng, "Data-driven prognostic scheme for bearings based on a novel health indicator and gated recurrent unit network," *IEEE Trans. Ind. Informat.*, early access, Apr. 26, 2022, doi: 10.1109/TII.2022.3169465.
- [4] N. E. Huang, Z. Shen, S. Long, M. Wu, H. Shih, Q. Zheng, N. Yen, C. Tung, and H. Liu, "The empirical mode decomposition and the Hilbert spectrum for nonlinear and non-stationary time series analysis," *Proc. Roy. Soc. London A*, vol. 454, no. 1971, pp. 903–995, 1998.
- [5] J. Zheng, J. Cheng, and Y. Yang, "Partly ensemble empirical mode decomposition: An improved noise-assisted method for eliminating mode mixing," *Signal Process.*, vol. 96, pp. 362–374, Mar. 2014.
- [6] H.-P. Huang, S.-Y. Wei, H.-H. Chao, C. F. Hsu, L. Hsu, and S. Chi, "An investigation study on mode mixing separation in empirical mode decomposition," *IEEE Access*, vol. 7, pp. 100684–100691, 2019.
- [7] Z. Wu and N. E. Huang, "Ensemble empirical mode decomposition: A noise-assisted data analysis method," *Adv. Adapt. Data Anal.*, vol. 1, no. 1, pp. 1–41, Jan. 2009.
- [8] X. Lang, N. ur Rehman, Y. Zhang, L. Xie, and H. Su, "Median ensemble empirical mode decomposition," *Signal Process.*, vol. 176, Nov. 2020, Art. no. 107686.
- [9] M. Guarascio and S. Puthusserypady, "Automatic minimization of ocular artifacts from electroencephalogram: A novel approach by combining complete EEMD with adaptive noise and Renyi's entropy," *Biomed. Signal Process. Control*, vol. 36, pp. 63–75, Jul. 2017.
- [10] Y. Pan, R. Hong, J. Chen, J. Singh, and X. Jia, "Performance degradation assessment of a wind turbine gearbox based on multi-sensor data fusion," *Mech. Mach. Theory*, vol. 137, pp. 509–526, Jul. 2019.
- [11] M. E. Torres, M. A. Colominas, G. Schlotthauer, and P. Flandrin, "A complete ensemble empirical mode decomposition with adaptive noise," in *Proc. IEEE Int. Conf. Acoust., Speech Signal Process. (ICASSP)*, May 2011, pp. 4144–4147.
- [12] S. Tian, X. Bian, Z. Tang, K. Yang, and L. Li, "Fault diagnosis of gas pressure regulators based on CEEMDAN and feature clustering," *IEEE Access*, vol. 7, pp. 132492–132502, 2019.
- [13] Y. Liu, L. Wang, L. Yang, X. Liu, and L. Wang, "Runoff prediction and analysis based on improved CEEMDAN-OS-QR-ELM," *IEEE Access*, vol. 9, pp. 57311–57324, 2021.
- [14] K. Dragomiretskiy and D. Zosso, "Variational mode decomposition," *IEEE Trans. Signal Process.*, vol. 62, no. 3, pp. 531–544, Feb. 2014.
- [15] Q. Chen, X. Lang, L. Xie, and H. Su, "Detecting nonlinear oscillations in process control loop based on an improved VMD," *IEEE Access*, vol. 7, pp. 91446–91462, 2019.
- [16] Q. Chen, J. Chen, X. Lang, L. Xie, N. U. Rehman, and H. Su, "Self-tuning variational mode decomposition," *J. Franklin Inst.*, vol. 358, no. 15, pp. 7825–7862, Oct. 2021.
- [17] S. Chen, X. Dong, Z. Peng, W. Zhang, and G. Meng, "Nonlinear chirp mode decomposition: A variational method," *IEEE Trans. Signal Process.*, vol. 65, no. 22, pp. 6024–6037, Nov. 2017.
- [18] Q. Chen, L. Xie, and H. Su, "Multivariate nonlinear chirp mode decomposition," *Signal Process.*, vol. 176, Nov. 2020, Art. no. 107667.
- [19] L. Latifoğlu, "The performance analysis of robust local mean mode decomposition method for forecasting of hydrological time series," *Iranian J. Sci. Technol., Trans. Civil Eng.*, vol. 46, no. 4, pp. 3453–3472, Jan. 2022.
- [20] J. S. Smith, "The local mean decomposition and its application to EEG perception data," *J. Roy. Soc. Interface*, vol. 2, no. 5, pp. 443–454, 2005.
- [21] L. Xie, X. Lang, J. Chen, A. Horch, and H. Su, "Time-varying oscillation detector based on improved LMD and robust Lempel–Ziv complexity," *Control Eng. Pract.*, vol. 51, pp. 48–57, Jun. 2016.
- [22] Z. Liu, Y. Jin, M. J. Zuo, and Z. Feng, "Time-frequency representation based on robust local mean decomposition for multicomponent AM-FM signal analysis," *Mech. Syst. Signal Process.*, vol. 95, pp. 468–487, Oct. 2017.
- [23] Y. Pan, H. Wang, J. Chen, and R. Hong, "Nonstationary signal de-noising method of slow-speed large-size slewing bearing using robust local mean decomposition," *Proc. SPIE*, vol. 12127, pp. 638–642, Dec. 2021.

- [24] L. Zhan, F. Ma, J. Zhang, C. Li, Z. Li, and T. Wang, "Fault feature extraction and diagnosis of rolling bearings based on enhanced complementary empirical mode decomposition with adaptive noise and statistical time-domain features," *Sensors*, vol. 19, no. 18, p. 4047, Sep. 2019.
- [25] S. Mirjalili, "Moth-flame optimization algorithm: A novel nature-inspired heuristic paradigm," *Knowl.-Based Syst.*, vol. 89, pp. 228–249, Nov. 2015.
- [26] Y. Wu, R. Chen, C. Li, L. Zhang, and Z. Cui, "Hybrid symbiotic differential evolution moth-flame optimization algorithm for estimating parameters of photovoltaic models," *IEEE Access*, vol. 8, pp. 156328–156346, 2020.
- [27] Y. Wu, R. Chen, C. Li, L. Zhang, and W. Dai, "An adaptive sine-cosine moth-flame optimization algorithm for parameter identification of hybrid active power filters in power systems," *IEEE Access*, vol. 8, pp. 156378–156393, 2020.
- [28] L. Wang and Y. Shao, "Fault feature extraction of rotating machinery using a reweighted complete ensemble empirical mode decomposition with adaptive noise and demodulation analysis," *Mech. Syst. Signal Process.*, vol. 138, Apr. 2020, Art. no. 106545.
- [29] H. Liu and J. Xiang, "A strategy using variational mode decomposition, L-Kurtosis and minimum entropy deconvolution to detect mechanical faults," *IEEE Access*, vol. 7, pp. 70564–70573, 2019.
- [30] B. Xu, F. Zhou, H. Li, B. Yan, and Y. Liu, "Early fault feature extraction of bearings based on Teager energy operator and optimal VMD," *ISA Trans.*, vol. 86, pp. 249–265, Mar. 2019.
- [31] H. Han, S. Cho, S. Kwon, and S.-B. Cho, "Fault diagnosis using improved complete ensemble empirical mode decomposition with adaptive noise and power-based intrinsic mode function selection algorithm," *Electronics*, vol. 7, no. 2, p. 16, 2018.
- [32] Y. Li, Y. Li, X. Chen, J. Yu, H. Yang, and L. Wang, "A new underwater acoustic signal denoising technique based on CEEMDAN, mutual information, permutation entropy, and wavelet threshold denoising," *Entropy*, vol. 20, no. 8, p. 563, Jul. 2018.
- [33] L.-Q. Zuo, H.-M. Sun, Q.-C. Mao, X.-Y. Liu, and R.-S. Jia, "Noise suppression method of microseismic signal based on complementary ensemble empirical mode decomposition and wavelet packet threshold," *IEEE Access*, vol. 7, pp. 176504–176513, 2019.
- [34] Y. Jiang, C. Li, Z. Yang, Y. Zhao, and X. Wang, "Remaining useful life estimation combining two-step maximal information coefficient and temporal convolutional network with attention mechanism," *IEEE Access*, vol. 9, pp. 16323–16336, 2021.
- [35] Y. Shen, W. Zheng, W. Yin, A. Xu, and H. Zhu, "Feature extraction algorithm using a correlation coefficient combined with the VMD and its application to the GPS and GRACE," *IEEE Access*, vol. 9, pp. 17507–17519, 2021.
- [36] Q. Fu, B. Jing, P. He, S. Si, and Y. Wang, "Fault feature selection and diagnosis of rolling bearings based on EEMD and optimized Elman_AdaBoost algorithm," *IEEE Sensors J.*, vol. 18, no. 12, pp. 5024–5034, Jun. 2018.
- [37] H. Wang, P. Wang, L. Song, B. Ren, and L. Cui, "A novel feature enhancement method based on improved constraint model of online dictionary learning," *IEEE Access*, vol. 7, pp. 17599–17607, 2019.
- [38] Y. Cheng, Z. Wang, B. Chen, W. Zhang, and G. Huang, "An improved complementary ensemble empirical mode decomposition with adaptive noise and its application to rolling element bearing fault diagnosis," *ISA Trans.*, vol. 91, pp. 218–234, Aug. 2019.
- [39] B. R. Bakshi, "Multiscale PCA with application to multivariate statistical process monitoring," *AICHE J.*, vol. 44, no. 7, pp. 1596–1610, Jul. 1998.
- [40] A. Graps, "An introduction to wavelets," *IEEE Comput. Sci. Eng.*, vol. 2, no. 2, pp. 50–61, Jun. 1995.
- [41] Y. Feng, X. Huang, R. Hong, and J. Chen, "Residual useful life prediction of large-size low-speed slewing bearings—A data driven method," *J. Vibroeng.*, vol. 17, no. 8, pp. 4164–4179, Dec. 2015.
- [42] M. Žvokelj, S. Zupan, and I. Prebil, "Multivariate and multiscale monitoring of large-size low-speed bearings using ensemble empirical mode decomposition method combined with principal component analysis," *Mech. Syst. Signal Process.*, vol. 24, no. 4, pp. 1049–1067, May 2010.
- [43] M. Žvokelj, S. Zupan, and I. Prebil, "Non-linear multivariate and multiscale monitoring and signal denoising strategy using kernel principal component analysis combined with ensemble empirical mode decomposition method," *Mech. Syst. Signal Process.*, vol. 25, no. 7, pp. 2631–2653, Oct. 2011.
- [44] G. Rilling, P. Flandrin, and P. Goncalves, "On empirical mode decomposition and its algorithms," in *Proc. IEEE Workshop Nonlinear Signal Image Process. (EURASIP)*, vol. 3, Jun. 2003, pp. 8–11.
- [45] Y.-T. Sheen, "A complex filter for vibration signal demodulation in bearing defect diagnosis," *J. Sound Vibrat.*, vol. 276, nos. 1–2, pp. 105–119, Sep. 2004.



YUBIN PAN received the B.S. and Ph.D. degrees from Nanjing Tech University, Nanjing, China, in 2014 and 2020, respectively. He was a Visiting Scholar with the Center for Intelligent Maintenance Systems (IMS), University of Cincinnati, Cincinnati, OH, USA, from 2018 to 2019. He is currently a Postdoctoral Fellow at the School of Mechanical and Power Engineering, Nanjing Tech University. His research interests include prognostics health management, smart manufacturing, and artificial intelligence.



ZONGQIU HU received the M.S. degree from the Huazhong University of Science and Technology, Hubei, China, in 2013. He is currently a Deputy Senior Engineer at China Three Gorges Construction Engineering Corporation. His research interests include new energy and hydropower project management.



JIE CHEN received the Ph.D. degree from the Nanjing University of Science and Technology, Nanjing, China, in 2005. She is currently a Full Professor at the School of Mechanical and Power Engineering, Nanjing Tech University. She is also the Director of the Mechatronics Research Institute, Nanjing Tech University, the Distinguished Expert of Jiangsu Provincial Commission of Economy and Information Technology, and the middle-aged and young academic leader of "Blue Project" of Jiangsu Provincial Department of Education. Her research interests include vibration signal processing theories and industrial process control and measurement. She is a reviewer for several SCI-indexed journals in this field.



HUA WANG received the B.S. and Ph.D. degrees in mechanical engineering from Harbin Engineering University, Harbin, China, in 2001 and 2006, respectively. He was a Visiting Scholar with the Department of Mechanical and Industrial Engineering, University of Massachusetts, USA, from 2014 to 2015. He is currently a Full Professor at the School of Mechanical and Power Engineering, Nanjing Tech University. His research interests include machinery condition monitoring and fault diagnosis, mechanical signal processing, intelligent fault diagnostics, and remaining useful life prediction. He is a Senior Member of the China Mechanical Engineering Society. He is also a reviewer for several SCI-indexed journals in this field.



RONGJING HONG received the Ph.D. degree from Southeast University, Nanjing, China, in 2006. He is currently a Full Professor at the School of Mechanical and Power Engineering, Nanjing Tech University. His current research interests include advanced CNC theory and digital manufacturing technology.